Dynamic Surrogate Model based Optimization for MPPT of Centralized Thermoelectric Generation Systems under Heterogeneous Temperature Difference

Xiaoshun Zhang, Bo Yang*, Tao Yu, and Lin Jiang,

***Abstract*—A novel dynamic surrogate model based optimization (DSMO) for centralized thermoelectric generation (TEG) system affected by heterogeneous temperature difference (HeTD) is designed to achieve maximum power point tracking (MPPT) in this paper. Since HeTD usually results in multiple local maximum power points (LMPPs), DSMO needs to rapidly approximate the global maximum power point (GMPP) instead of being trapped at a low quality LMPP. To avoid a blind search, a radial basis function network is adopted to construct the dynamic surrogate model of input/output feature according to the real-time data of centralized TEG system. Furthermore, a greedy search is adopted to accelerate the convergence based on dynamic surrogate model. Four case studies are undertaken to evaluate the practicability and superiority of the proposed method compared with that of a single LMPP based MPPT method and three common meta-heuristic algorithms. In addition, the implementation feasibility of DSMO is demonstrated by the hardware-in-the-loop (HIL) experiment based on dSpace platform**

***Index Terms*—thermoelectric generation system, maximum power point tracking, heterogeneous temperature difference, dynamic surrogate model, greedy search**

I. INTRODUCTION

THERMOELECTRIC generation (TEG) system has become a promising generation technology for energy saving and sustainability, which is a device that is capable of producing electricity from wasted heat [1]. The merits of TEG system are simple structure, high reliability, low weight, long lifetime, as well as eco-friendliness [2]. Hence, TEG system is promising for various practical applications, e.g., automotive waste heat recovery [3], combined heat and power system [4], energy efficient buildings [5], natural gas boiler [6], etc.

Due to its inherent low efficiency, maximum power point tracking (MPPT) is a crucial task for the optimal operation of TEG system [7]. The idea of MPPT is originated from solar energy where PV panels are exposed at various solar irradiations thus many MPPT techniques are developed to seek the maximum power point (MPP) affected different operation conditions. In particular, MPPT strategies can be categorized into traditional and intelligent approaches [8].

Perturb and observe (P&O) [9] and incremental conductance (INC) [10] are two common MPPT strategies for TEG systems which have low-cost and high stability. Moreover, an open-circuit voltage (OCV) approach was proposed to improve power generation efficiency because the voltage on the load is half of the open-circuit voltage [11]. And reference [12] employed fractional short-circuit current (SCC) to realize MPPT which needs to regular measure the short-circuit current. Furthermore, work [13] designed a linear extrapolation-based MPPT strategy to obtain MPP which only requires three sampling cycles. Furthermore, literature [14] developed an extreme seeking control (SEC) approach which can successfully seek the extremum of steady-state online optimization under the unknown circumstance.

Nevertheless, the aforementioned MPPT techniques are merely available for the scenario with only single local maximum power point (LMPP) under homogeneous temperature difference (HoTD). In practice, centralized TEG configuration is a very cost-effective choice in industry which combines all TEG modules together and connected with just one converter [15]. In fact, each parallel series of TEG modules will generate a single power output peak under different temperature inputs, in which the peak value and corresponding control solution will vary as the temperature inputs change. Hence, the centralized TEG system with multiple parallel series of TEG modules will result in multiple power output peaks in the presence of heterogeneous temperature difference (HeTD), like the PV systems when influenced by partial shading condition (PSC) [16,17]. Under such condition, the single LMPP based MPPT algorithms may have a high probability to be trapped at one low-quality LMPP with a bad initial control solution, such that the overall generation efficiency becomes very low.

To approximate the global maximum power point (GMPP) from the multiple LMPPs, the meta-heuristic algorithms [18] are the better solutions due to their high application flexibility and strong global search ability. For example, genetic algorithm (GA) [19] and particle swarm optimization (PSO) [20], while various meta-heuristic algorithms are successfully utilized to realize MPPT for PV systems affected PSC. Hence, they are also suitable to approximate the GMPP for centralized TEG system affected HeTD considering their similarities in essence. However, they generally employ a population with multiple individuals to implement the global exploration and local exploitation to approximate GMPP, in which a part of individuals is usually adopted for a random search. Consequently, they often consume a long computation time for MPPT and easily results in a large power fluctuation due to the random search. To handle these issues, the surrogate model based optimization [21] is a frequently-used method which can

construct a computationally cheap model for acquiring an approximate fitness value instead of an exact value obtained from the real system associated with relatively large computational burden. Hence, based on such advantage, a new dynamic surrogate model based optimization (DSMO) is proposed for MPPT of centralized TEG system under HeTD. And the main advantages of DSMO are given as follows:

● Compared with the conventional approaches based on single LMPP, DSMO is able to seek the GMPP more effectively instead of being trapped into a low-quality LMPP via constructing a radial basis function meshwork based dynamic surrogate model for the input/output (I/O) relation of centralized TEG system.

● DSMO can implement a more efficient guided search instead of a blind search by the greedy search based on the dynamic surrogate model compared to meta-heuristic methods. Besides, DSMO only employs a single individual instead of a population with multiple individuals for MPPT, which can dramatically reduce the computation time with much less global exploration and local exploitation.

II. TEG System Modelling

A. TEG Module Modelling

The equivalent circuit of a TEG module is demonstrated in Fig. 1. The open-circuit voltage V_{oc} produced by TEG module is described by [22]

$$V_{oc} = \alpha_{pn}\left(T_h - T_c\right) = \alpha_{pn}\Delta T \tag{1}$$

where α_{pn} represent the Seebeck coefficient; T_h is the temperature of hot side; T_c is the temperature of cold side; and ΔT means the temperature diversity between the T_h and T_c.

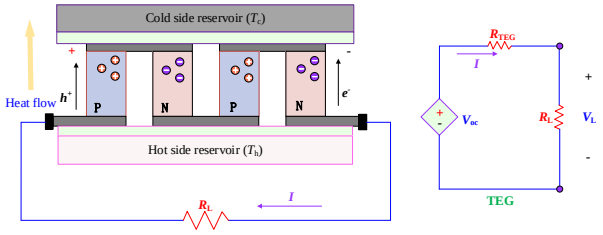

Fig. 1. Circuit diagram of a TEG module.

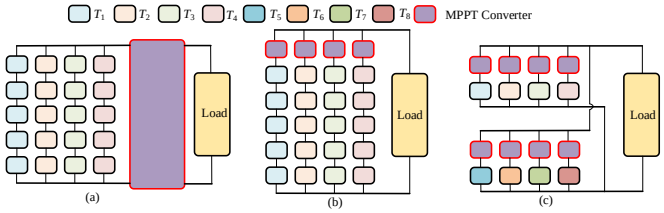

Fig. 2. Three TEG system structures. (a) centralized, (b) string-type, and (c) modularized.

Normally, Seebeck effect and Thomson effect have important influence on TEG system. And the Thomson coefficient τ is described by [10]

$$\tau = T\frac{d\alpha_{pn}}{dT} \tag{2}$$

Hence, the more accurate Seebeck coefficient can be obtained with the change of mean temperature T, which is expressed as [23]:

$$\alpha_{pn}(T) = \alpha_0 + \alpha_1 \ln\left(T/T_0\right) \tag{3}$$

where α_0 is the fundamental character of α_{pn}; α_1 is the variation rate of τ; and T_0 is the temperature reference.

Based on the circuit theory, the output power generated by TEG module is illustrated by

$$P_{TEG} = \left(\alpha_{pn}\Delta T\right)^2 \cdot \frac{R_L}{\left(R_L + R_{TEG}\right)^2} \tag{4}$$

where P_{TEG} denotes the power output of TEG module; R_{TEG} and R_L are the internal resistance and load resistance of TEG module, respectively.

B. Structure of TEG System

In order to produce sufficient power output to satisfy specific practical applications, several TEG modules are usually connected in different configurations to establish an whole TEG system. Due to the increased size and scale of such integrated TEG system, it

is often exposed at HeTD which results in noticeable mismatched power losses [14]. Figure 2 illustrates three common TEG system structures [15], as (a) centralized TEG structure which is consisted of several TEG modules in series and parallel with a MPPT converter; (b) string-type TEG structure which lets TEG string along isothermal line of heat source and each string has a MPPT converter; (c) modularized TEG structure which provides each TEG module with an independent MPPT converter so as to track its own MPP.

And this paper aims to design DSMO based MPPT approach for centralized TEG structure as its simple construction and satisfactory hardware cost.

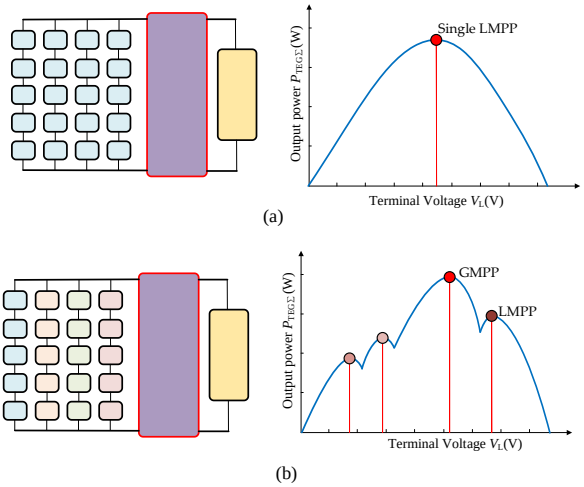

Fig. 3. Power-voltage characteristics of centralized TEG system affected by HoTD and HeTD. (a) HoTD and (b) HeTD.

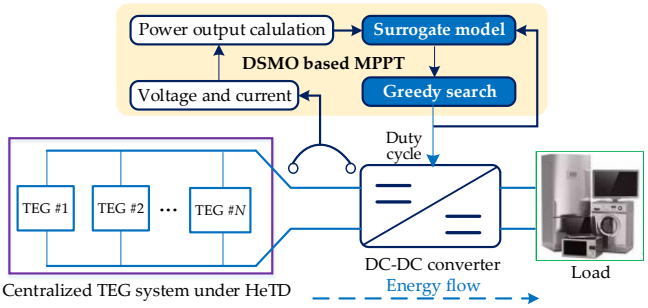

Fig. 4. Control framework of DSMO based MPPT of centralized TEG system.

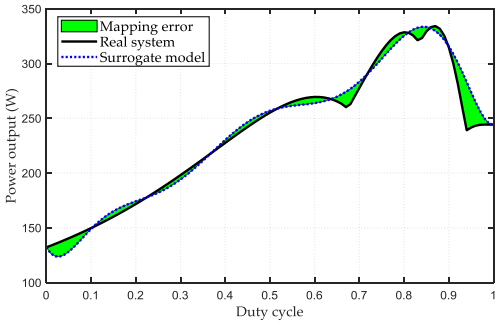

Fig. 5. Illustration of mapping relationship by surrogate model.

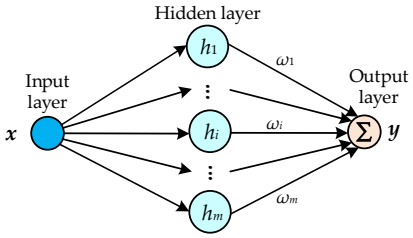

Fig. 6. Illustration of RBF network based surrogate model for MPPT.

C. TEG System Modelling Affected by HeTD

TEG modules often connected in series and/or parallel to obtain the desired power. And the output current of the *i*th TEG module can be calculated by [31]

$$I_i = \begin{cases} \left(V_{\text{oc}}^i - V_{\text{L}}^i\right) \cdot \dfrac{I_{\text{sc}}^i}{V_{\text{oc}}^i} = I_{\text{sc}}^i - \dfrac{V_{\text{L}}^i}{R_{\text{TEG}}^i}, & \text{if } 0 \le V_{\text{L}}^i \le \dfrac{I_{\text{sc}}^i}{V_{\text{oc}}^i} \\ 0, & \text{otherwise} \end{cases} \tag{5}$$

where $V_{\text{oc}}{}^i$ and $I_{\text{sc}}{}^i$ are the open-circuit voltage and short-circuit current of the *i*th TEG module, respectively; $V_{\text{L}}{}^i$ and $R_{\text{TEG}}{}^i$ are the terminal voltage and internal resistance of the *i*th TEG module, respectively. The output power generated by the *i*th TEG module is

$$P_{\text{TEG}}^i = \begin{cases} V_{\text{L}}^i \cdot I_i = I_{\text{sc}}^i V_{\text{L}}^i - \dfrac{I_{\text{sc}}^i}{R_{\text{TEG}}^i} \cdot \left(V_{\text{L}}^i\right)^2, & \text{if } 0 \le V_{\text{L}}^i \le \dfrac{I_{\text{sc}}^i}{V_{\text{oc}}^i} \\ 0, & \text{otherwise} \end{cases} \tag{6}$$

Then, all the output power of the centralized TEG system can be obtained as

$$P_{\text{TEG}} = \sum\nolimits_{i=1}^{N} P_{\text{TEG}}^i \tag{7}$$

It is very crucial to analyse the relationship between P_{TEG} and terminal voltage V_{L} of converter of centralized TEG system, as shown in Fig. 3. Here, multiple LMPPs and only one GMPP appear under HeTD, while MPPT controller attempts to effectively seek GMPP.

III. MPPT BASED ON DSMO FOR CENTRALIZED TEG SYSTEM

A. Control Framework

In general, the energy of load is provided by TEG system via a DC-DC converter [10], as illustrated in Fig. 4. Consequently, the V_{L} can be updated by change the duty cycle [22] of pulse-width modulation (PWM) signal to the DC-DC converter. This means that DSMO needs to search an optimal duty cycle to obtain the GMPP. In this paper, DSMO mainly contains two operations. Firstly, a surrogate model will be dynamically updated according to the real-time implemented duty cycle and the corresponding steady power output. Then, a greed search will be implemented to rapidly acquire a high-quality duty cycle for the next control interval according to the current surrogate model. Finally, DSMO based MPPT can gradually approximate GMPP through repeating the above two operations.

B. Radial Basis Function Network based Surrogate Model

The proposed surrogate model aims to discover the mapping relationship between the power output and the duty cycle according to the real-time collected operation data of centralized TEG system, as illustrated in Fig. 5. In fact, various methods can construct such surrogate model. Since it is a single input single output mapping, a radial basis function (RBF) meshwork [24] is adopted because its excellent nonlinear mapping ability and fast convergence. In essence, a RBF meshwork is a three-layer feed-forward meshwork [25] (See Fig. 6), including an input layer, an output layer, and a hidden layer, upon which the desired power output can be calculated by

$$f^{\text{SM}}(x) = y(x) = \sum\nolimits_{i=1}^{m} \omega_i h_i(x) \tag{8}$$

where f^{SM} denotes the mapping function of the surrogate model; x is the input of RBF, i.e., the duty cycle; h_i means the primary function of the *i*th hidden neuron; m represents the hidden neurons number; and ω_i means the coefficient between the *i*th hidden neuron and the output.

C. Greedy Search

Based on the dynamic surrogate model (8), DSMO can approximate GMPP under desired control accuracy. To further accelerate the convergence, the searching range is designed to be gradually shrinked as the iteration number increases, as follows:

$$x_{k+1} = \max_{lb_k \le x \le ub_k} f_k^{\text{SM}}(x) \tag{9}$$

$$\begin{cases} lb_k = x_k^{\text{best}} / \left(k_{\max} + 1 - k\right) \\ ub_k = x_k^{\text{best}} + \left(1 - x_k^{\text{best}}\right) / k \end{cases} \tag{10}$$

where k denotes the kth iteration; x_{k+1} is the duty cycle at the (k+1)th iteration; $x_k{}^{\text{best}}$ represents the current best solution at the kth iteration so far; lb_k and ub_k denote the lower and upper limitations of the searching range, respectively; and $k_{\max}$ denote the scheduled maximum iteration number.

TABLE I
THE EXECUTION PROCEDURE OF DSMO BASED MPPT OF TEG SYSTEM.

1: Initialize the algorithm parameters and the inputs of training samples by Eq. (11);

2: Set k:=1;
3: **FOR** i:=1 to n
4: Implement the duty cycle of the ith training sample in the DC-DC converter;
5: Collect the real-time voltage and current outputs of centralized TEG system;
6: Calculate the desired output of the ith training sample by Eq. (12);
7: **END FOR**
8: **WHILE** $k \le k_{max}$
9: Construct the surrogate model via training RBF network;
10: Update the lower and upper bounds of the searching range by Eq. (10);
11: Determine the minimum number of discrete searching points by Eq. (14);
12: Implement the greedy search by Eq. (8)-(9);
13: Implement the new duty cycle of PWM signal ;
14: Collect the real-time voltage and current outputs of centralized TEG system;
15: Calculate the actual power output corresponding to the current duty cycle by Eq. (12);
16: Add the new training sample to the surrogate model;
17: Set k:=k+1;
18: **END WHILE**
19: 20: Output the best duty cycle of the PWM signal;
20: Repeat step 1 to step 19 if the input temperatures vary.

TABLE II
THE EXECUTION PROCEDURE OF GENERAL META-HEURISTIC ALGORITHMS BASED MPPT OF TEG SYSTEM.

1: Initialize the algorithm parameters and population;
2: Set k:=1;
3: **WHILE** $k \le k_{max}$
4: **FOR** j:=1 to J
5: Implement the new duty cycle of the jth individual to the DC-DC converter;
6: Collect the real-time voltage and current outputs of centralized TEG system;
7: Calculate the fitness value of the jth individual according to the actual power output;
8: **END FOR**
9: Determine the roles for all the individuals according to their fitness values;
10: **FOR** j:=1 to J
11: Update the solution of the jth individual according to its searching operation;
12: **END FOR**
13: Set k:=k+1;
14: **END WHILE**
15: Output the optimal duty cycle of the PWM signal to the DC-DC converter;
16: Re-execute the optimization from step 1 to step 15 when the input temperatures change.

D. Specific Design for MPPT

a) Design of dynamic surrogate model

The property of surrogate model is primary depend on the training data and the design of RBF network. In fact, there are infinite possible distribution of temperature for the system, such that the number of LMPPs and their corresponding duty cycles cannot be known in advance. Under this situation, if the training data is designed to be intensive within a small range, then the surrogate model cannot provide a highly accurate output mapping for other ranges of duty cycles. As a result, it easily traps into an LMPP near the initial range and is difficult to approximate the GMPP. Therefore, the initial training data should be designed to be spread from its lower to upper limits, thereby the surrogate model can closely approximate the curve between the power output and duty cycle over the whole range. Hence, all the potential LMPPs can be discovered as much as possible based on the surrogate model. Consequently, the duty cycles of the training data are selected uniformly within its lower and upper limits, as follows:

$$x_i^0 = \frac{1}{2n} + \frac{i-1}{n}, \quad i = 1, 2, ..., n \tag{11}$$

where x_i^0 denote the duty cycle of the ith initial training sample; and n is training samples number, in which the initial number of training samples is represented by n_0. In general, a larger n_0 will lead to a high mapping accuracy and a high generalization for the surrogate model. However, it will consume more computation time to acquire and accomplish the training of RBF network, which also easily result in a large energy loss and a large power fluctuation for centralized TEG system during acquiring the training data. Hence, n_0 should be set to be a proper value for the specific centralized TEG system.

After accomplishing different duty cycles to the DC-DC converter, the outputs of training data can be obtained via the stable voltage and current outputs, as follows:

$$\hat{y}_i = V_{\mathrm{TEG}}^{\mathrm{out}}\left(x_i\right) \cdot I_{\mathrm{TEG}}^{\mathrm{out}}\left(x_i\right) \tag{12}$$

where $\hat{y}_i$ is the actual power output of the ith training sample, i.e., the desired output of RBF network; $V_{\mathrm{TEG}}^{\mathrm{out}}\left(x_i\right)$ and $I_{\mathrm{TEG}}^{\mathrm{out}}\left(x_i\right)$ are the steady voltage and current outputs of the centralized TEG system after implementing the duty cycle x_i, respectively.

Note that the training data of building the surrogate model is acquired from the online operating results of centralized TEG system. In order to make DMSO continuously approximate the GMPP under various operating points, the surrogate model will be rebuilt with the new training data in each MPPT task with the fixed temperature inputs. As the temperature inputs change, the previous training data will be cleaned up, while DSMO will be re-executed to approximate the new GMPP with the updated training data.

Here, a frequently-used Gaussian function [25] has been utilized as the fundamental function of RBF network, which can be written as

$$h_i = \exp\left(-\frac{\|x - c_i\|^2}{2\sigma_i^2}\right), \quad i = 1, 2, ..., n \tag{13}$$

where c_i is the middle of ith hidden neuron and σ_i denotes the breadth of Gaussian function for the ith hidden neuron.

To accomplish the training of RBF network, this paper adopts an exact design [26] to determine the centers, weights, and the number of hidden neurons based on the training samples and the given width.

b) Design of greedy search

Note that x_{k+1} in Eq. (9) can be determined via exploring a finite number of uniform discrete points between the lower and upper bounds, which completely depends on the desired control accuracy. Hence, the number of discrete searching points should satisfy the following condition, as

$$\frac{ub_k - lb_k}{n_d} \le \delta \tag{14}$$

where δ is the desired control accuracy and n_d represents the number of discrete searching points in greedy search.

c) Implementation process

To sum up, Table I presents the entire MPPT implementation process of DSMO for the centralized TEG system affected HeTD. In the initial phase, DSMO only requires a small number (i.e., initial number of training samples n_0) of global exploration. Then it can implement the deep local exploitation with greedy search based on the dynamic surrogate model, which also requires a smaller number of local exploitation (i.e., k_{max}). Hence, it only requires (n_0+k_{max}) control time cycles to finish the optimization for each MPPT task with the fixed temperature inputs. In contrast, the meta-heuristic algorithms generally employ a population with multiple individuals for MPPT, in which each individual needs to occupy a control time cycle to acquire the power output from the centralized TEG system in each iteration. According to the updated fitness values of all the individuals, each meta-heuristic algorithm can determine their roles and update their solutions according to their searching operations, as illustrated in Table II. Therefore, each meta-heuristic algorithm requires (J×k_{max}) control time cycles to finish the optimization, in which J is the population size. As a result, DSMO will consume less computation time than the general meta-heuristic algorithms to search a high-quality optimum for MPPT. Furthermore, it also causes a slight impact on the memory and processing as the number of training data increases from n_0 to (n_0+k_{max}).

Note that DSMO needs to continuously update the dynamic surrogate model, as shown in Step 9 of Table I. Under an MPPT task, the dynamic surrogate model of DSMO needs to reconstruct itself every control time cycle within the maximum iterations number k_{max}, i.e., it requires k_{max} reconstructions in each MPPT task. On the other hand, as the input temperatures change, it needs to re-execute the optimization process with k_{max} reconstructions of dynamic surrogate model, as illustrated in Table I. Finally, this work assumes that the input temperatures of centralized TEG system can be collected with the specific temperature sensor, thus the temperature changes can be identified.

IV. Case Studies

For the purpose of testing the MPPT performance of DSMO for centralized TEG system affected HeTD, four cases are undertaken in this section. The TEG model is the centralized TEG configuration (See Fig. 2(a)), while each string can be modelled as a voltage source with an internal resistance, as shown in Fig. 1. Table III gives the main parameters of centralized TEG system and the connected DC-DC converter, where the main parameters of each TEG module are referred from the practical parameters in [22, 23]. Besides, the comparison algorithm includes P&O [9], PSO [20], whale optimization algorithm (WOA) [27], and grey wolf optimizer (GWO) [28]. In order to fairly compare all the meta-heuristic approaches, the size of population and the maximum number of iterations they utilize are totally same, which are designed as 5 and 6, respectively. Hence, each meta-heuristic algorithm requires 30 (5×6) control time cycles to finish the optimization. Besides, the fixed step size of P&O is set as 0.005, while the main parameters of DSMO is provided in Table IV via trial-and-error. As shown in Table III, the testing centralized TEG system only contains four parallel strings, such that the number of LMPPs is up to four. Hence, ten initial training samples is enough to effectively generalize many possible operating points for each MPPT task in case studies. What's more, the control period of all approaches is set as 0.01s, such that a new duty cycle will be updated by each approach and the voltage and current will be produced of centralized TEG system in every 0.01s. All the simulations are implemented on Matlab/Simulink 2017b through a personal computer with an Intel^R CoreTMi7 CPU at 1.8 GHz and 16 GB of RAM.

TABLE III
PARAMETERS OF CENTRALIZED TEG SYSTEM AND DC-DC CONVERTER.

Centralized TEG system		DC-DC converter	
String number	4	Transfer function	$V_{out}=V_{in}/(1-D_C)$
Module number of each string	200	Switching frequency	20 kHz
Basic part of Seebeck coefficient	210 μV/K	Load	3 Ω
Variation rate of Seebeck coefficient	120 μV/K	Inductance	250 mH
Reference temperature	300 /K	Capacitance	66/200 μF

TABLE IV
PARAMETERS OF DSMO

n_0	δ	k_{max}	σ
10	0.0001	10	1

Besides, two variables are introduced to achieve a quantitative power oscillation evaluation of centralized TEG system, as follows [16,17]:

$$\Delta v^{\text{avg}} = \frac{1}{T-1}\sum_{t=2}^{T}\frac{\left|P_{\text{out}}(t)-P_{\text{out}}(t-1)\right|}{P_{\text{out}}^{\text{avg}}} \tag{15}$$

$$\Delta v^{\text{max}} = \max_{t=2,3,\ldots,T}\frac{\left|P_{\text{out}}(t)-P_{\text{out}}(t-1)\right|}{P_{\text{out}}^{\text{avg}}} \tag{16}$$

where Δv^{avg} and Δv^{max} are the mean and the maximum variability of the output power, respectively; t represents the time period indicatrix; T denotes the number of the entire time period; and $P_{\text{out}}^{\text{avg}}$ represents the average output power of centralized TEG system during all the time period.

A. Output Characteristics of Centralized TEG System

To analyze the influence of temperature difference on the open circuit voltage and internal resistance of TEG string, the hot side temperature of string #1 is designed to vary from 50 ℃ to 250 ℃, while the cold side temperature is set to be constant (40 ℃). As shown in Fig. 7, it is clear that a larger temperature difference can lead to a larger open circuit voltage and internal resistance. As a result, it will cause different output characteristics between different strings with different input temperatures, thus the multiple peaks of power output will be occurred. To verify this feature, the hot side temperatures of four TEG strings (#1 to #4) are designed as 247 ℃, 123 ℃, 76 ℃, and 41 ℃, respectively; and the cold side temperatures are set to be 47 ℃, 31 ℃, 18 ℃, and 13 ℃, respectively. Fig. 8 provides the *I-V* and *P-V* curves of all the strings. Firstly, it shows that the output current decreases as the output voltage increases, in which the descent rate of string #4 is the highest due to its smallest temperature difference input. Secondly, it can be found that the P-V curves of all the strings are the downward parabolas with single peak, where the peak value and the corresponding voltage increase as the temperature difference input increase. Consequently, the curve of total power output easily leads to multiple peaks, as the four peaks shown in Fig. 8(b).

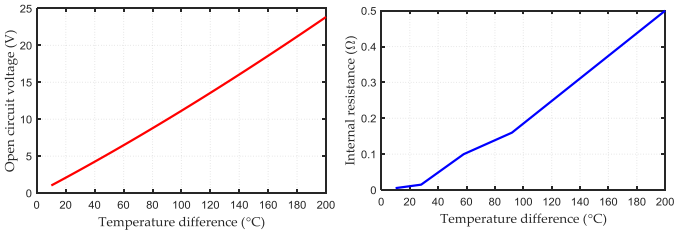

(a) (b)

Fig. 7. Influence of temperature difference on the generation parameters of TEG string #1. (a) Open circuit voltage and (b) Internal resistance.

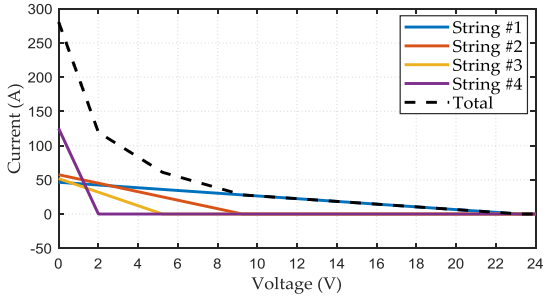

(a)

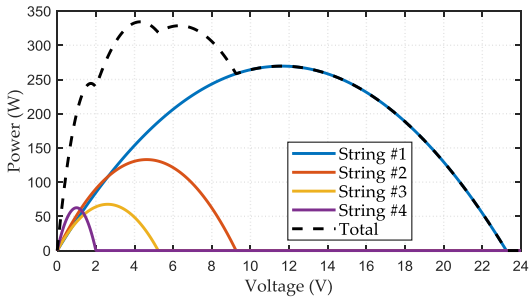

(b)

Fig. 8. Output characteristic of centralized TEG system. (a) *I-V* curves and (d) *P-V* curves.

B. Start-Up Test

The purpose of this section is to validate the MPPT performance of DSMO at start-up (from zero point) affected HeTD, where the hot side temperatures of four TEG strings are designed as 247 ℃, 123 ℃, 76 ℃, and 41 ℃, respectively; and the cold side temperatures are designed to be 47 ℃, 31 ℃, 18 ℃, and 13 ℃, respectively. The equivalent parameters of each string are provided in Table VI.

The simulation results achieved by five methods for the centralized TEG system as shown in Fig. 9. One can easily found that the energy output obtained by P&O is much smaller than that obtained by other methods since it is designed for approximating the single LMPP under HoTD in Fig. 9(d). Meanwhile, since all the three meta-heuristic algorithms possess strong global search ability, thus they can finally converge to the MPPs with high quality. Moreover, the proposed DSMO is able to make the TEG system to produce the largest output energy under HeTD among all the methods. Besides, all the meta-heuristic approaches can easily result in a obvious power fluctuation for the reason of their random operation based global search. In contrast, P&O can result in a much smaller power oscillation because of its simple and fixed control strategy. Besides, DSMO also can seek an excellent MPP with inconspicuous power fluctuation, which results from the surrogate model based greedy search that can implement a guided efficient search instead of a blind random search.

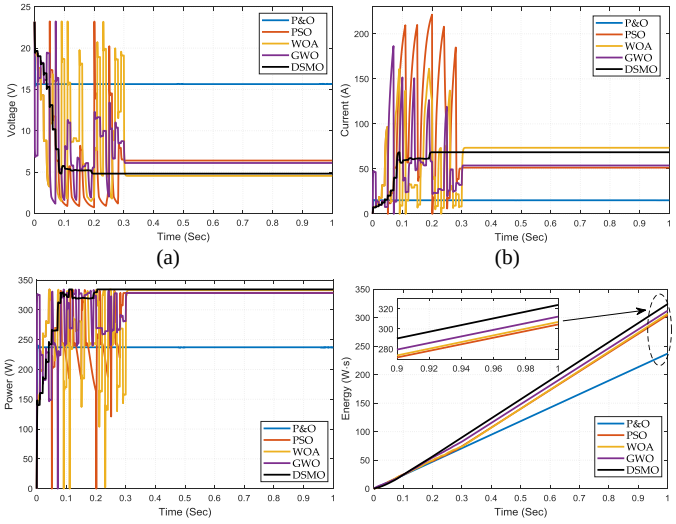

Fig. 9. MPPT results acquired by five methods in the start-up test. (a) Voltage, (b) Current, (c) Power, and (d) Energy.

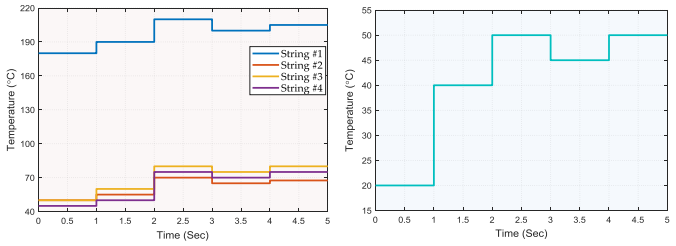

Fig. 10. Step varayion of temperature inputs. (a) Cold side and (b) Hot side.

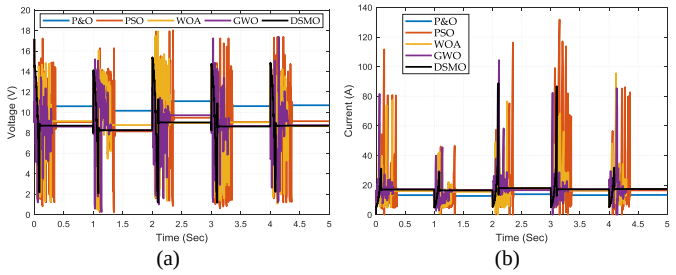

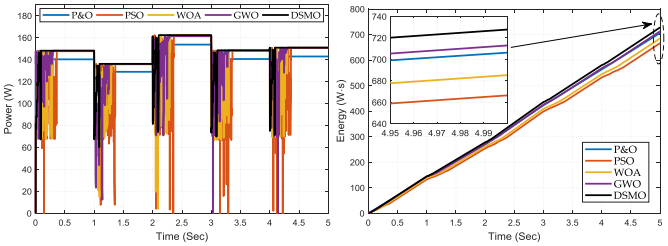

(c) (d)

Fig. 11. MPPT results acquired by five methods in the step test. (a) Voltage, (b) Current, (c) Power, and (d) Energy.

C. Step Variation of Temperature

This test applies a set of temperature steps (see Fig. 10) to verify the MPPT performance of DSMO. And as shown in Fig. 10(a), the temperature inputs of the cold side are set to be the identical change curves for the whole strings. Like a typical TEG waste heat recovery system, the cold side temperature can be maintained constant by cooling water in practice [29], while the heat side temperature is determined by the exhaust energy. The accurate values of temperature inputs for each string are given in Table VII.

Figure 11 provides the MPPT results of five approaches under above environment. Significantly, P&O owns the smallest power oscillations while DSMO generates the largest energy outputs. This also demonstrates that conventional MPPT methods based on single LMPP affected HeTD cannot distinguish LMPPs and GMPP, while the RBF network based surrogate model can achieve a highly accurate mapping between the power output and the duty cycle for the centralized TEG system. Moreover, the meta-heuristic algorithms still cause a large power fluctuation since they easily find an inferior solution with a random operation. In contrast, P&O also make the TEG system operate at a steady MPP with a faster speed. Meanwhile, DSMO leads to a much smaller power fluctuation during the searching process, which verifies that the dynamic surrogate model based greedy search can effectively avoid an inferior solution and significantly accelerate the convergence.

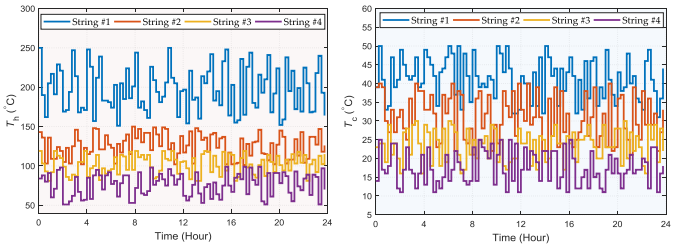

Fig. 12. Random variation of temperature inputs. (a) Cold side and (b) Hot side.

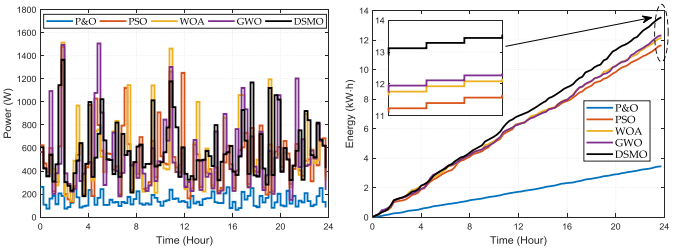

(a) (b)

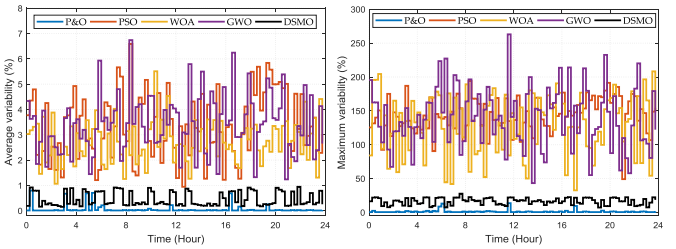

(c) (d)

Fig. 13. MPPT results of TEG system obtained by five methods in the random test. (a) Voltage, (b) Current, (c) Power, and (d) Energy.

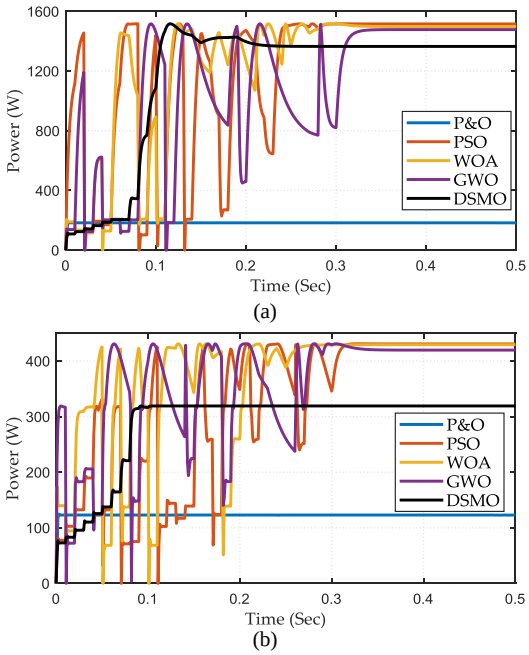

Fig. 14. Dynamic process of power outputs obtained by five methods for two scenarios in random temperature variation. (a) 8th scenario and (b) 60th scenario.

TABLE V
STATISTICAL RESULTS ACQUIRED BY FIVE APPROACHES

Scenarios	Indices	P&O	PSO	WOA	GWO	DSMO
Start-up	Energy (W s)	237.02	304.47	306.97	312.28	**323.94**
	Δv^{max} (%)	**0.50**	102.44	106.99	69.63	10.26
	Δv^{avg} (%)	**0.01**	1.07	1.45	0.80	0.09
Step variation	Energy (W s)	706.26	666.39	685.26	712.97	**727.80**
	Δv^{max} (%)	**13.62**	106.67	76.54	90.34	55.06
	Δv^{avg} (%)	**0.01**	1.55	1.06	0.67	0.22
Random change	Energy (kW h)	3.45	11.66	12.16	12.33	**13.55**
	Δv^{max} (%)	**1.33**	144.36	130.47	139.62	16.57
	Δv^{avg} (%)	**0.06**	3.37	2.74	3.42	0.46
Computation time (s)		**0.01**	0.30	0.30	0.30	0.20

D. Random Temperature Change

In this test, each string of the centralized TEG system will undergo random temperature change during one day, and the time change period is set as 15 minutes (see Fig. 12). Hence, it consists of 96 scenarios with different temperature inputs in 24 hours, in which the temperature inputs of each string in some scenarios are given in Table VIII.

Figure 13 illustrates the MPPT results acquired by five approaches under acquired. In most of time, Fig. 13(a) can effectively demonstrate that DSMO can obtain a larger output power compared with that of other methods. However, DSMO also traps into a low-quality LMPP in some scenarios, e.g., the 8th and 60th scenarios. Fig. 14 gives the dynamic process of power outputs obtained by five methods for these two scenarios. It can be clearly found that each meta-heuristic algorithm can converge to a high-quality LMPP although they cause a large power fluctuation. In contrast, DSMO rapidly converge to a low-quality LMPP due to the over fitting with a small number of training samples. The power output obtained by P&O is the smallest among all the methods for each time cycle because the effect of HeTD. Again, DSMO can geenrate the largest energy output among all the methods, as shown in Fig. 13(b). In terms of average variability and maximum variability, P&O with simple and fixed control strategy can result in the smallest power fluctuation for centralized TEG system under HeTD, as illustrated in Fig. 13(c)-(d). Similarly, DSMO owns a quite small average and maximum variability than that of three meta-heuristic algorithms, which effectively validates its high optimization stability with the dynamic surrogate model based greedy search.

E. Discussion of Statistical Results

Table V illustrates the statistical outcomes acquired by five approaches under above tests, in which the optimal values of various indices are highlighted in bold; and the computation time is the time to converge to a stable operation point for each MPPT task with fixed temperature inputs. From the comparison of energy outputs of all approaches, DSMO can get the largest energy outputs under above scenarios for centralized TEG system. For instance, in the random temperature change, which is 393.10%, 116.24%, 111.42%, and 109.93% to that of P&O, PSO, WOA, and GWO, respectively. Moreover, both the average and maximum change of P&O are the smallest among all the methods under all the scenarios although it merely obtains the smallest energy outputs, while its computation time is the shortest due to its simple control rule. With the less computation time, DSMO is able to considerably reduce the power fluctuations from the comparisons of average and maximum variabilities compared with meta-heuristic algorithms, while its average variability is only 6.09% of that obtained by WOA in the start-up test. Hence, GSDD can

simultaneously approximate the GMPP and guarantee a small power fluctuation via a guided efficient search.

F. Sensitivity Analysis

The temperature ratios from 0% to 100% (5% change separation) are adopted to study the sensitivity [30-34] between temperature inputs and power outputs for centralized TEG system affected HeTD. And the 100% reference temperature of the hot side and cold side is same as start-up test. Figure 15 gives the sensitivity results of average power output, average variability, and maximum variability under different temperature ratios obtained by five methods. Figure 15(a) illustrates a positive relationship between the temperature inputs and the power outputs, i.e., as temperature proportion raising, the generated power increases correspondingly. For the meta-heuristic algorithms, both the average variability and maximum variability randomly change as the temperature ratio increases, which mainly results from their random operation based global search. In contrast, both of them obtained by P&O are basically constant under different temperature ratios. Compared with other methods, the average variability and maximum variability acquired by DSMO decrease when the temperature ratio is smaller than 30%, while they are basically unchanged when the temperature ratio is larger than 30%, which also verifies the high convergence stability of DSMO.

V. HIL EXPERIMENT

An HIL experiment based on dSpace platform can effectively validate the practicability of different MPPT approaches while the configuration and experiment platform are demonstrated in Fig. 16. Moreover, the centralized TEG system (1)-(7) is embedded on DS1006 platform while the sampling frequency is designed to be f_s=100 kHz. Moreover, MPPT based on DSMO (8)-(14) is carried out on DS1104 platform while the sampling frequency is designed to be f_c=1 kHz.

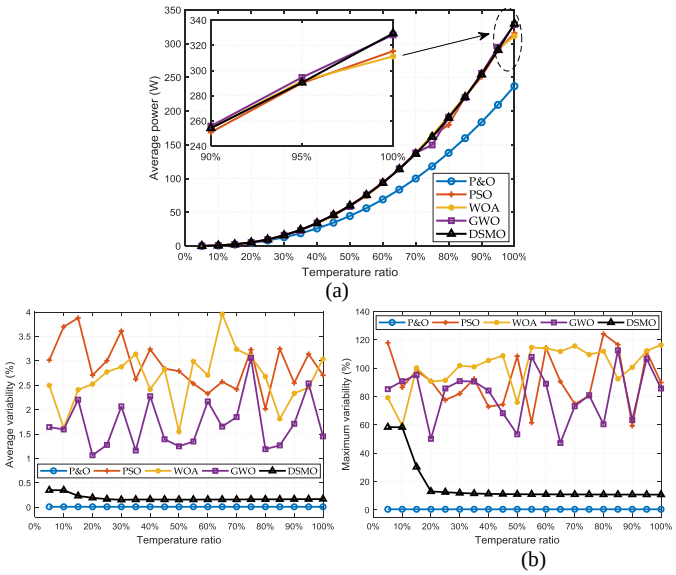

Fig. 15. Sensitivity results of temperature inputs obtained by five methods. (a) Average power output, (b) Average variability, and (c) Maximum variability.

A. HIL Experiment Results of Start-Up Test

Figure 17 makes a comparison between the simulation and HIL experiment outcomes acquired by start-up test. It can be easily found that the similarity of their results is very high.

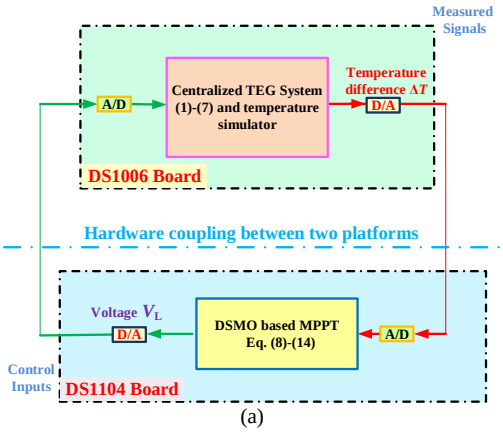

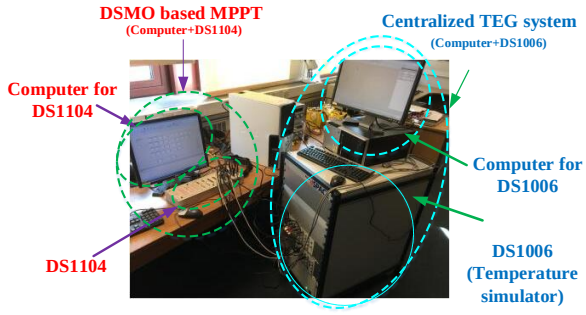

(b)

Fig. 16. The structure and hardware platform of HIL experiment. (a) configuration and (b) platform.

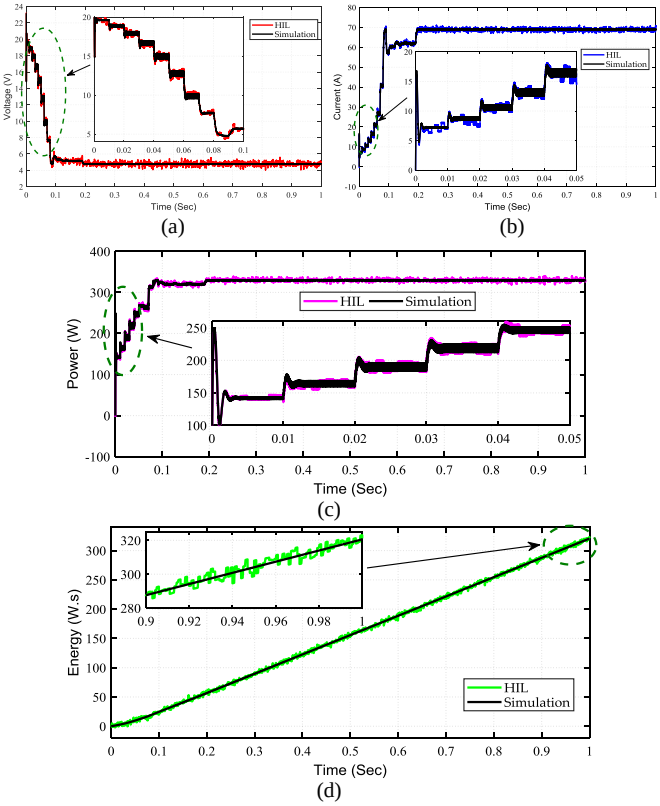

(a) (b) (c) (d)

Fig. 17. MPPT performance comparison between simulation and HIL under the start-up test. (a) Voltage, (b) Current, (c) Power, and (d) Energy.

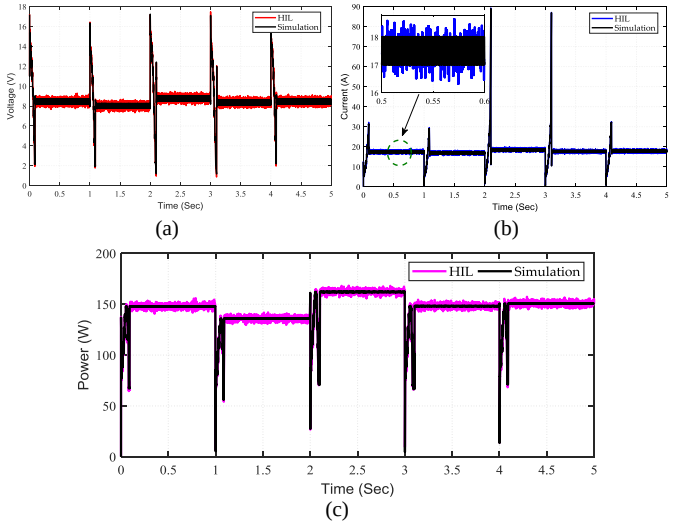

(a) (b) (c)

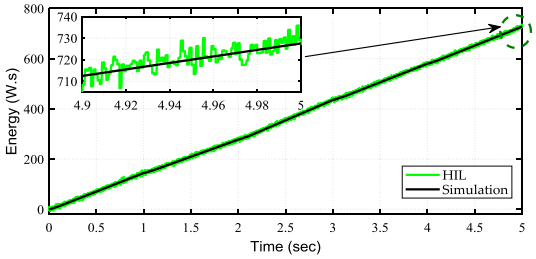

(d)

Fig. 18. MPPT performance comparison between simulation and HIL under the step change of temperature. (a) Voltage, (b) Current, (c) Power, and (d) Energy.

B. HIL Experiment Results of Step Variation of Temperature

Fig. 18 depicts the outcomes of simulation and HIL experiment acquired under step variation of temperature. Clearly, their responses are quite close.

VI. Conclusion

A new MPPT strategy based on DSMO for centralized TEG system under HeTD is proposed in this paper while the major contributions are summarized as follows:

(1) The MPPT strategy based on DSMO is designed for centralized TEG system with satisfactory hardware cost, such that the dissipative energy during the industrial/domestic process is able to effectively reuse and recycle.

(2) In contrast with single LMPP based MPPT methods, e.g., P&O, DSMO can distinguish LMPPs and GMPP for centralized TEG system under HeTD. And DSMO can noticeably reduce the power fluctuations via implementing an efficient guided search instead of a random search compared to meta-heuristic methods.

(3) A series of comprehensive experiments, such as case studies and a dSpace based HIL experiment are carried out to prove the validity of DSMO. Simulation results clearly demonstrate that DSMO can effectively produce the highest output energy under various scenarios among all the methods, e.g., 393.10%, 116.24%, 111.42%, and 109.93% to that of P&O, PSO, WOA, and GWO in the test of random temperature change. In addition, it can also lead to a much slighter power fluctuation than that of the meta-heuristic approaches.

Although DSMO can rapidly converge to an optimum with a small power fluctuation, it is also easy to trap into a low-quality LMPP in some operating scenarios. To address this limitation, one of our future works will focus on another efficient mapping technique to construct the dynamic surrogate model, which can not only require a small number of training samples, but also effectively avoid the over fitting.

Appendix

TABLE VI
EQUIVALENT PARAMETERS OF EACH STRING IN START-UP TEST

Parameter	String #1	String #2	String #3	String #4
V_{oc} (V)	24.04	10.05	6.03	2.80
R_{TEG} (Ω)	0.50	0.16	0.10	0.015

TABLE VII
TEMPERATURE INPUTS OF EACH STRING IN STEP CHANGE TEST

Temperature	Time (s)	String #1	String #2	String #3	String #4
Hot side (℃)	0 to 1	180	50	50	45
	1 to 2	190	55	60	50
	2 to 3	210	70	80	75
	3 to 4	200	65	75	70
	4 to 5	205	67.5	80	75
Cold side (℃)	0 to 1	20	20	20	20
	1 to 2	40	40	40	40
	2 to 3	50	50	50	50
	3 to 4	45	45	45	45
	4 to 5	50	50	50	50

TABLE VIII
TEMPERATURE INPUTS OF EACH STRING IN SOME SCENARIOS OF RANDOM TEMPERATURE VARIATION

Temperature	No. of scenario	String #1	String #2	String #3	String #4
Hot side (℃)	4	205	136	81	91
	8	221	119	110	98
	12	247	125	89	62
	16	171	123	119	57
	20	212	147	114	95
	24	181	127	94	92
	28	205	117	114	78
	32	201	150	95	53
	36	171	142	108	63
	40	194	140	86	81
	44	250	121	107	96

	48	195	138	105	90
	52	184	103	110	76
	56	205	136	119	73
	60	195	123	99	64
	64	164	117	116	75
	68	236	135	110	83
	72	180	130	89	82
	76	210	115	87	51
	80	224	127	113	91
	84	195	108	94	66
	88	169	143	104	69
	92	169	137	108	89
	96	164	126	115	70
Cold side (℃)	4	33	30	19	16
	8	41	31	20	12
	12	41	36	21	17
	16	40	38	16	21
	20	42	32	28	11
	24	47	32	19	21
	28	50	38	21	19
	32	35	28	21	14
	36	40	28	24	23
	40	36	29	28	13
	44	50	34	17	11
	48	33	40	28	11
	52	34	29	18	22
	56	32	22	25	22
	60	44	39	29	22
	64	43	32	26	11
	68	41	27	25	12
	72	46	31	25	22
	76	36	32	29	11
	80	34	23	28	20
	84	48	25	20	17
	88	35	25	23	17
	92	41	29	25	23
	96	44	33	22	18

REFERENCES

[1] B. Yang, J.T. Wang, X.S. Zhang, M.T. Zhang, H.C. Shu, S.N. Li, T.Y. He, L. Yang, and T. Yu, "MPPT design of centralized thermoelectric generation system using adaptive compass search under non-uniform temperature distribution condition", *Energy Convers. Manage.* vol. 199, 111991, Nov. 2019.

[2] V. S. Krishna, N. H. Md, and S. M. A. Mohamed, "Methodological reviews and analyses on the emerging research trends and progresses of thermoelectric generators," *Int. J.* Energy *Res.*, vol. 43, pp. 113-140, Jan. 2019.

[3] Q.-M. Cao, W.-L. Luan, and T.-C. Wang, "Performance enhancement of heat pipes assisted thermoelectric generator for automobile exhaust heat recovery," *Appl. Therm. Eng.*, vol. 130, pp. 1472-1479, Feb. 2018.

[4] A. Montecucco, J. Siviter, and A. R. Knox, "Combined heat and power system for stoves with thermoelectric generators," *Appl. Energy*, vol. 185, pp. 1336-1342, Jan. 2017.

[5] I. Kashif, H. Khairul, R. Saidur, M. W. Kareem, and B. S. Bidyut, "Study of thermoelectric and photovoltaic facade system for energy efficient building development: A review," *J. Cleaner Prod.*, vol. 209, pp. 1376-1395, Feb. 2019.

[6] Y.-L. Zhao, S.-X. Wang, M.-H. Ge, Y.-Z. Li, and Z.-J. Liang, "Analysis of thermoelectric generation characteristics of flue gas waste heat from natural gas boiler," *Energy Conv. Manag.*, vol. 148, pp. 820-829, Sep. 2017.

[7] B. Yang, M.T. Zhang, X.S. Zhang, J.B. Wang, H.C. Shu, S.N. Li, T.Y. He, L. Yang, and T. Yu, "Fast atom search optimization based MPPT design of centralized thermoelectric generation system under heterogeneous temperature difference", *J. Cleaner Prod.* vol. 248, 119301, Mar. 2020.

[8] S.-J. Wu, S. Wang, C.-J. Yang, and K.-R. Xie, "Energy management for thermoelectric generators based on maximum power point and load power tracking," *Energy Conv. Manag.*, vol. 177, pp. 55-63, Dec. 2018.

[9] C. Yu and K.-T. Chau, "Thermoelectric automotive waste heat energy recovery using maximum power point tracking," *Energy Conv. Manag.*, vol. 50, no. 6, pp. 1506-1512, Jun. 2009.

[10] S. Twaha, J. Zhu, Y. Yan, and B. Li, "Performance analysis of thermoelectric generator using dc-dc converter with incremental conductance based maximum power point tracking," *Energy Sustain Dev.*, vol. 37, pp. 86-98, Apr. 2017.

[11] A. Montecucco and A.R. Knox, "Maximum power point tracking converter based on the open-circuit voltage method for thermoelectric generators," *IEEE Trans. Power Electron.*, vol. 30, no. 2, pp. 828-839, Mar. 2015.

[12] I. Laird and D. D. C. Lu, "High step-up DC/DC topology and MPPT algorithm for use with a thermoelectric generator," *IEEE Trans. Power Electron.*, vol. 28, no. 7, pp. 3147-3157, Jul. 2013.

[13] B. Bijukumar, A. G. K. Raam, G. S. Ilango, and C. Nagamani, "A linear extrapolation based MPPT algorithm for thermoelectric generators under dynamically varying temperature conditions," *IEEE Trans. Energy Convers.*, vol. 33, no. 4, pp. 1641-1649, Dec. 2018.

[14] N. Phillip, O. Maganga, K. Burnham, M. A. Ellis, S. Robinson, and J. Dunn, "Investigation of maximum power point tracking for thermoelectric generators," *J. Electron. Mater.*, vol. 42, no. 7, pp. 1900-1906, Jul. 2013.

[15] T. Rakesh and R.S.N. Edward, "Investigation of thermoelectric generators connected in different configurations for micro-grid applications," *Int. J. Energy Res.*, vol. 42, no. 2, pp. 2290-2301, May. 2018.

[16] B. Yang, T. Yu, X.-S. Zhang, H.-F. Li, H.-C. Shu, Y.-Y. Sang, and L. Jiang, "Dynamic leader based collective intelligence for maximum power point tracking of PV systems affected by partial shading condition," *Energy Conv. Manag.*, vol. 179, pp. 286-303, Jan. 2019.

[17] B. Yang, L.-E. Zhong, T. Yu, H.-F. Li, X.-S. Zhang, H.-C. Shu, Y.-Y. Sang, and L. Jiang, "Novel bio-inspired memetic salp swarm algorithm and application to MPPT for PV systems considering partial shading condition," *J. Cleaner Prod.*, vol. 215, pp. 1203-1222, Apr. 2019.

[18] H. Rezk, A. Fathy, and A. Y. Abdelaziz, "A comparison of different global MPPT techniques based on meta-heuristic algorithms for photovoltaic system subjected to partial shading conditions," *Renew. Sustain. Energy Rev.*, vol. 74, pp. 377-386, Jul. 2017.

[19] S. Daraban, D. Petreus, and C. Morel, "A novel MPPT (maximum power point tracking) algorithm based on a modified genetic algorithm specialized on tracking the global maximum power point in photovoltaic systems affected by partial shading," *Energy*, vol. 74, pp. 374-388, Sep. 2014.

[20] H. Li, D. Yang, W.-Z. Su, J.-H. Lü, and X.-H. Yu, "An overall distribution particle swarm optimization MPPT algorithm for photovoltaic system under partial shading," *IEEE Trans. Ind. Electron.*, vol. 66, no. 1, pp. 265-275, Jan. 2019.

[21] Z.-Z. Zhou, Y. S. Ong, P. B. Nair, A. J. Keane, and K. Y. Lum, "Combining global and local surrogate models to accelerate evolutionary optimization," *IEEE Trans. Syst., Man, Cybern., C* Appli. *Rev*., vol. 37, no.1, pp. 66-76, Jan. 2007.
[22] Y.-H. Liu, Y.-H. Chiu, J.-W. Huang, and S.-C. Wang, "A novel maximum power point tracker for thermoelectric generation system" *Renew. Energy,* vol. 97, pp. 306-318, Nov. 2016.
[23] A. Chakraborty, B. B. Saha, S. Koyama, and K. C. Ng, "Thermodynamic modelling of a solid state thermoelectric cooling device: Temperature-entropy analysis," *Int. J. Heat Mass Transfer*, vol. 49, no. 19-20, pp. 3547-3554, Sep. 2006.
[24] R. G. Regis, "Evolutionary programming for high-dimensional constrained expensive black-box optimization using radial basis functions," *IEEE Trans. Evol. Comput.*, vol. 18, no. 3, pp. 326-347, Jun. 2014.
[25] J.-M. Lian, Y.-G. Lee, S. C. Sudhoff, and S. H. Zak, "Self-organizing radial basis function network for real-time approximation of continuous-time dynamical systems," *IEEE Trans. Neural Networks*, vol. 19, no. 3, pp. 460-474, Mar. 2008.
[26] M. H. Beale, M. T. Hagan, and H. B. Demuth. Neural network toolboxTM user's guide. The MathWorks, Natick, 2018.
[27] N. Kumar, I. Hussain, B. Singh, and B. K. Panigrahi, "MPPT in dynamic condition of partially shaded PV system by using WODE technique," *IEEE Trans. Sustain. Energy*, vol. 8, no. 3, pp. 1204-1214, Jul. 2017.
[28] B. Yang, X.S. Zhang, T. Yu, H.C. Shu, Z.H. Fang, "Grouped grey wolf optimizer for maximum power point tracking of doubly-fed induction generator based wind turbine," *Energy Conv. Manag.* vol. 133, pp. 427-443, Feb. 2017.
[29] D. Ji, Z. Wei, S. Mazzoni, M. Mengarelli, S. Rajoo, J. Zhao, J. Pou, and A. Romagnoli, "Thermoelectric generation for waste heat recovery: Application of a system level design optimization approach via Taguchi method," *Energy Convers. Manage.*, vol. 172, pp. 507-516, Sep. 2018.
[30] B. Yang, T. Yu, H.C. Shu, J. Dong, L. Jiang, "Robust sliding-mode control of wind energy conversion systems for optimal power extraction via nonlinear perturbation observers," *Applied Energy*, vol. 210, pp. 711-723, Jan. 2018.
[31] B. Dasu, M. Sivakumar, R. Srinivasarao, "Interconnected multi-machine power system stabilizer design using whale optimization algorithm," *Pro. Control Mod. Power Syst.* vol. 4, no. 4, pp. 13-23, Apr. 2019.
[32] B. Yang, T. Yu, H.C. Shu, Y.M. Zhang, J. Chen, Y.Y. Sang, L. Jiang, "Passivity-based sliding-mode control design for optimal power extraction of a PMSG based variable speed wind turbine," *Renew. Energy*, vol. 119, pp. 577-589, Apr. 2018.
[33] B. Yang, L. Jiang, L. Wang, W. Yao, Q.H. Wu, "Nonlinear maximum power point tracking control and model analysis of DFIG based wind turbine ," *Int. J. Electr. Power Energy Syst.* vol. 74, pp. 429-436, Jan. 2016.
[34] T. S. L. V. Ayyarao, "Modified vector controlled DFIG wind energy system based on barrier function adaptive sliding mode control," *Pro. Control Mod. Power Syst.*, vol. 4, no. 4, pp. 34-41, Feb. 2019.